Iraqi Journal of Physics, 2024
https://doi.org/10.30723/ijp.v22i3.1259
Vol. 22, No. 3, PP. 93-105
P-ISSN: 2070-4003
E-ISSN: 2664-5548

Green Synthesis of CuO Nanoparticles Mediated Rhazya Stricta Plant Leaves Extract Characterization and Evaluation of their Antibacterial and Anticancer Activity (in vitro Study)

Abeer M. Muslim[1,2a*] and Iqbal S. Naji[1b]
[1] *Department of Physics, College of Science, University of Baghdad, Baghdad, Iraq*
[2]*Ibn Sina University of Medical and Pharmaceutical Sciences, Baghdad, Iraq*
[b]E-mail: iqbalnaji78@gmail.com
[a*]Corresponding author: abeer94mohammed@gmail.com

Abstract

In this study, a straightforward, expeditious, and environmentally friendly approach to synthesize copper oxide nanoparticles (CuONPs) utilizing an aqueous extract of Rhazya Stricta (R. stricta) leaves was employed. The CuONPs underwent various analytical techniques for characterization, including X-ray diffractometer (XRD), field emission scan electron microscope (FESEM), energy dispersive X-ray (EDX) analyses, UV-Vis spectroscopy, Fourier transform infrared spectroscopy (FTIR), and zeta potential. The XRD analysis authenticated the monoclinic crystal nature, revealing an average crystallite size of 15.6 nm. FESEM images depicted semi-spherical and cubic shapes, with particle sizes ranging from 56.64 to 86.95 nm. The formation of CuONPs was initially confirmed by the observable change in color, attributed to the excitation of surface Plasmon resonance at 280 nm in the UV-Vis spectra. FTIR analysis affirmed the presence of functional groups in the R. Stricta leaves extract, serving as both reducing and stabilizing agents, facilitating the formation of CuONPs. Zeta potential measurements indicated substantial stability with a value of -49.7 mV. The biosynthesized CuONPs were further evaluated for their antibacterial properties against Klebsiella Pneumoniae (K. pneumoniae) and Staphylococcus aureus (S. aureus), yielding inhibition zones of 21 mm and 30 mm, respectively. Additionally, the cytotoxicity assessment of CuONPs against A549 cell lines revealed higher cytotoxicity of 81.47 ± 1.517 at a CuONP concentration of 100 µg/ml. This work is the first attempt at R. stricta-facilitated synthesis of CuONPs as antibacterial and anticancer agents. It can subsequently be exploited as a potential candidate for these agents and might be utilized further in vivo studies.

Article Info.

Keywords:
CuO, Nanoparticles, Rhazya Stricta, Antibacterial Activity, Anticancer Activity.

Article history:
Received: Mar.07, 2024
Revised: Jun. 17, 2024
Accepted: Jun. 30, 2024
Published: Sep.01, 2024

1. Introduction

Nanotechnology, a rapidly advancing field, is experiencing significant growth through advanced technologies, focusing on constructing and applying nano-scale materials within the 1 to 100 nm range. Recently, due to the widespread environmental pollution affecting the world, an increased utilization of green technology and chemistry has been adopted to synthesize nanoparticles. Nanomaterials, particularly clusters of metal and oxide atoms or molecules, achieved through the utilization of plant extracts have captured considerable attention from scientific communities due to their unique nanostructures [1, 2]. The creation of nanoparticles involves various synthesis processes, including the synthesis of dry particles and the dispersion of nanoparticles in liquid. Nanostructures can be formed by assembling atoms or reducing the size of microparticles [3] through two main approaches: the top-down, breaking down bulk materials into nano-sized structures, and the bottom-up, building materials from molecule to molecule. Top-down methods face challenges with surface imperfections, while bottom-up approaches provide precise control over particle size, leading to

favourable properties. Nanoparticle synthesis methods are categorized into physical, chemical, and biological processes; physical and chemical approaches have drawbacks, such as difficulty in achieving narrow size, high costs, and environmental concerns [4-7]. The biological method, linked to green chemistry, is favored for its eco-friendly, cost-effective nature; it involves using organisms like algae, plants [8], bacteria [9], yeast [10], fungi [11], and human cells [12] to convert metal ions into specific nanoparticles. The green synthesis method has gained considerable attention from nanotechnology researchers, who consider it a new decisive key. Plants/microbial resources have been used to fabricate copper oxide nanoparticles (CuONPs) [13]. Also, the synthesis of copper oxide nanoparticles (CuONPs) from various plant parts, such as leaves [14], peels [15], and seeds [16], is well-established. These plant parts contain different concentrations and combinations of phytochemicals that act as reducing agents. CuO has garnered significant interest as it represents the most straightforward member within the family of copper compounds, exhibiting numerous advantageous physical properties, such as high-temperature superconductivity, electron correlation effects, and spin dynamics [17, 18]. The utilization of CuONPs is rising across diverse applications, including catalysis, batteries, gas sensors, heat transfer fluids, and solar energy [19]. The crystal structures of CuO possess a narrow band gap, contributing to valuable photocatalytic and photovoltaic properties [20]. Recently, significant attention has been directed towards the escalating use of CuONPs as a substitute for antibiotics, owing to their distinct advantages over conventional antimicrobial agents [21]. Industries, particularly textiles, have harnessed the antimicrobial potential of these products to safeguard against microbial contamination. Green-synthesized nanoparticles have been employed to counteract textile-resistant microorganisms' growth, addressing nanoparticle toxicity concerns [22, 23].

Lung cancer, a challenging disease and a leading global cause of mortality accounts for 12.4% of new cases and 17.6% of deaths, according to previous studies [24]. Critical determinants of lung cancer risk, including smoking, lack of physical activity, alcohol consumption, and notably, air pollution, contribute to increased cancer-related mortality. Ineffective diagnostics and therapeutic interventions amplify cancer fatalities [25]. Chemotherapeutic drugs are seldom employed for treatment purposes due to their significant side effects, such as neuronal damage, disruption of normal cells, and skin irradiation. Consequently, there is a pressing need to develop environmentally friendly CuONPs as a non-toxic, cost-effective strategy for cancer treatment. Metal nanoparticles exhibit cytotoxicity by generating Reactive Oxygen Species (ROS), causing damage to proteins, membrane lipids, and cellular structures [26].

In this work, CuONPs were successfully synthesized using extract from Rhazya stricta (R. stricta) plant leaves. R. stricta is a species belonging to the Apocynaceae family. The leaves show many promising biological activities, e.g., antibacterial [27], antioxidant and anticancer activities [28]. We are the first to report its antibacterial and anticancer activities. Characterization was done using various analysis techniques. Finally, antibacterial and cytotoxic effects were also evaluated. Antibacterial activity was done against two bacterial strains (Staphylococcus aureus and Klebsiella pneumoniae). The cytotoxicity was evaluated by MTT assay against A549 cell lines.

2. Experimental Part

2.1. Materials

Copper nitrate (Cu $(NO_3)_2 \cdot 3H_2O$) was purchased from Thomas Baker, India. Sodium hydroxide pellets AR (NaOH) of a 98% purity were purchased from

labachemie, India. The Muller–Hinton agar medium was purchased from HiMedia, India. High purity Ethanol 99% was purchased from Duksan, Korea.

2.2. Plant Collection and Preparation of the Extract

R. stricta was imported in January from Ras al-Khaimah, of the United Arab Emirates. The leaves were cleaned three times under tap water and then again with deionized water (DW) to remove dust. The leaves were dried for a month in the shade at room temperature, after which they were pulverized into a fine powder using an electric mixer. 10 g of this powder was mixed with 500 ml of DW and heated to 80 °C for two hours. After a colored solution was created, the mixture was filtered through filter paper and centrifuged to remove any remaining impurities. The solution was kept refrigerated.

2.3. Preparation of CuONPs

The precursor solution was prepared by dissolving 5 g of copper nitrate in 150 ml of DW with stirring on a magnetic stirrer for half an hour, 100 ml of R. Stricta extract was added under magnetic mixing for one hour at 80˚C. 7.5 M of sodium hydroxide (NaOH) dissolved in 20 ml of DW was added dropwise to the precursor solution to adjust its pH to 12. The color of the solution turned from blue to dark green, which is the first sign of CuONPs formation. The solution was centrifuged, and the precipitation was separated and washed with DW and ethanol. Finally, the clean precipitation was dried at 75 °C for 3h to remove impurities. The calcination process was carried out at 600°C for 2h. The final product was black powder.

2.4. Characterization

CuONPs were examined with an X-ray diffractmeter (XRD, panalytical Xpert, UK) with Cu Kα radiation monochromatic filter in the range of 20˚-80˚. The morphology, particle size, and size distribution of the synthesized CuONPs were studied using a field emission scan electron microscope (FESEM- Imaging-EDS-Maping-line-EBSD/Germany). The presence of functional groups or identification of chemical bonding in CuONPs was evaluated using Fourier transform infrared spectroscopy (FTIR/ATR/Far-IR/ Near-IR Thermo Fisher Scientific USA). The optical properties of CuONPs were analyzed using UV-Visible spectrophotometer (UV-2550 Shimadzu, Japan) within the 100–1100 nm wavelength range. The surface charge and stability were determined by a zeta potential instrument (DLS/Zeta Malvern/ Zeta sizer, UK).

2.5. Antibacterial Activity

Using an agar-well diffusion assay, the antibacterial potential of the synthesized CuONPs synthesized using R. stricta leaves extract was examined against gram-positive and gram-negative bacterial strains. Muller-Hinton (MH) agar, about 20 ml, was aseptically added to sterile Petri dishes. Using a sterile wire loop, the bacterial species were extracted from their stock cultures. Using a sterile point, 6 mm-diameter wells were bored onto the agar plates following the culture of the bacteria. Various concentrations of CuONPs (100, 200, 400, and 800) μg/ml were added to the bored wells. The test bacteria were incubated overnight at 37°C before measuring and recording the average zones of inhibition diameter.

2.6. MTT Assays

The MTT assay was carried out using 96-well plates to ascertain the cytotoxic effect of CuONPs on A549 cell lines. 1×10^4 cells per well were used to seed the cell

line. Cells were treated with CuONPs at varying concentrations once a confluent monolayer formed, which took place after 24 hrs. Following a 48-hour treatment period, the media was removed, 28 µl of a 2 mg/ml MTT solution was added, and the cells were incubated for 2.5 hrs at 37°C to determine the viability of the cells. Following the removal of the MTT solution, 130 µl of DMSO (dimethyl sulphoxide) was added to the wells to solubilize the residual crystals. This was followed by a 15 minute shake-free incubation period at 37 °C. Three duplicates of the experiment were carried out, and the absorbency was measured at 492 nm using a microplate reader. The percentage of cytotoxicity, or the inhibition rate of cell growth, was computed using the following formula:

$$\text{Inhibition rate}\,(\%) = \frac{\mathrm{A} - \mathrm{B}}{\mathrm{A}} \times 100 \qquad (\mathbf{1})$$

where A represents the control's optical density and B represents the samples' optical density. A digital camera attached to an inverted microscope was used at × 40 magnification for imaging while the cells were being examined.

2.7. Statistical Analysis

GraphPad Prism 6 was used to perform the statistical analysis of the acquired data using an unpaired t-test. The data was displayed as the average ± standard deviation of three measurements.

3. Results and Discussion

FESEM analysis was used to investigate the morphology of CuONPs. The FESEM images of the CuONPs synthesized using R. stricta leaves extract are shown in Fig. 1 (a and b) with two different magnifications1µm and 500nm, respectively. The figure indicated that the NPs were agglomerated in clusters with semi-spherical and cubic structures. The particle size ranged from 56.64 to 86.95 nm. The agglomeration of CuONPs occurred as a result of many factors, such as high surface energy, surface area, surface tension, surface reactivity, the viscosity properties of the plant extract, attraction between the NPs, and oxidation of metal oxide NPs [29]. The form and morphology of the nanoparticles also rely on the reducing agent and stabilizing agent, which are derived from R. stricta leaves extract. Therefore, the semi-spherical morphology of the nanoparticles is attributed to the favorable selection of these agents. This conclusion is consistent with recent research by Pakzad et al. on the biosynthesis of CuONPs [30].

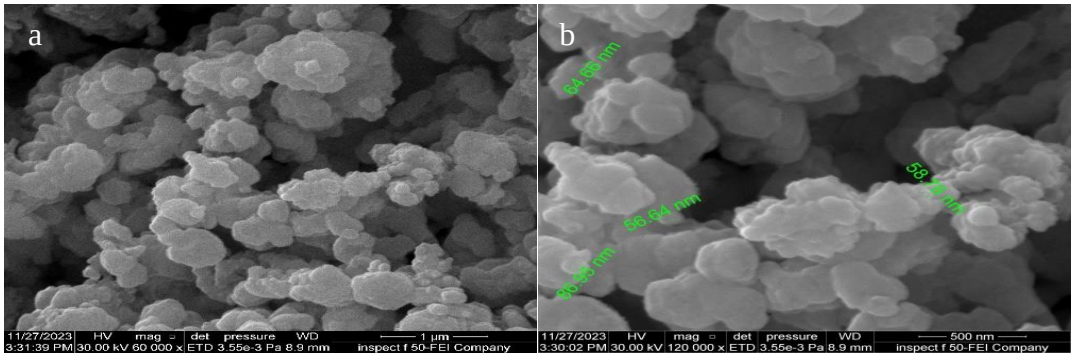

Figure 1: (a and b) low and high magnification FESEM images of the synthesized CuONPs.

Fig. 2 consolidates the EDX spectra and elemental composition of CuONPs. The production of oxide NPs is confirmed by three peaks for Cu and one for O in Fig. 2, which show their respective compositions of 78.1% and 21.9%. These results are in good agreement with Atri et al. [31].

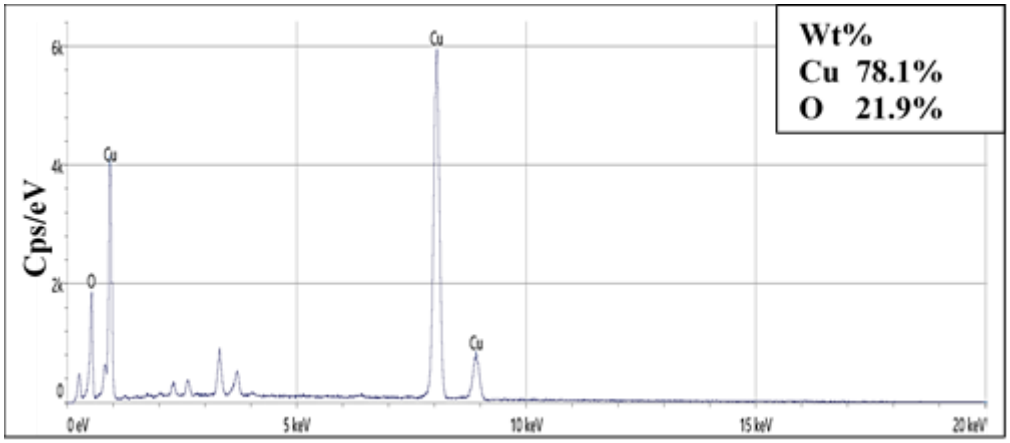

Figure 2: EDX pattern of CuONPs.

Fig. 3 shows the XRD pattern for CuONPs synthesized using R. stricta leaves extract. This figure revealed diffraction angles at 32.32˚, 35.32˚, 38.54˚, 46.07˚, 48.57˚, 53.26˚, 58.04˚, 61.33˚, 66.09˚, 67.79˚, 72.15˚ and 74.87˚ corresponding to miller induces planes (110), (-111), (111), (-112), (-202), (020), (202), (-113), (-311), (113), (311) and (004), respectively. The strongest diffraction angles were at 2θ=35.32˚ and 38.54˚. It was found that the CuONPs' diffraction pattern had peaks that were the same as the standard data from the JCPDS card no. 01-080-0076. This validates the development of a crystalline structure with a monoclinic shape. The average size of the crystals was determined by applying the Debye-Scherrer formula [32-34], and the resulting values are presented in Table 1.

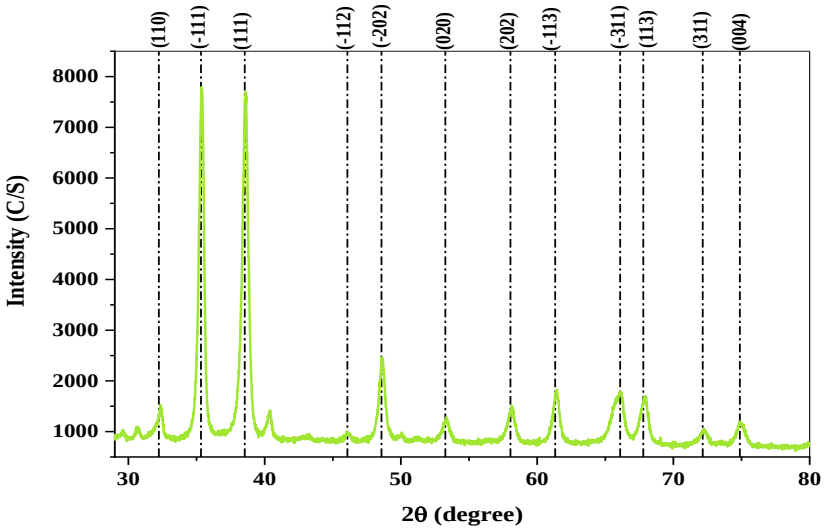

Figure 3: XRD pattern of CuONPs synthesized using R. stricta leaves extract.

$$D = \frac{K\lambda}{\beta COS\theta} \qquad (2)$$

where: D stands for the crystal size of CuONPs, k is factor shape (with a value of 0.9), λ the wavelength of X-ray, which is (1.541A), the Bragg diffraction angle is (θ), and β is

the Full-Width at Half Maximum (FWHM) of the diffraction peak. The mean crystallite size of CuONPs was found to be 15.6nm. A similar result was reported by Naika et al. [35]. The XRD pattern of the synthesized CuONPs showed clear and distinct reflections, which proves that the CuONPs have a crystalline structure, and no additional peaks were observed [36].

Table 1: Structural parameters of CuONPs synthesized using R. Stricta leaves extract.

2θ (degree)	$d_{hkl\ (exp.)}$	FWHM (degree)	hkl	D(nm)
32.2389	2.77445	0.6232	(110)	10.6
35.3282	2.53858	0.4076	(-111)	19.2
38.5432	2.33391	0.2475	(111)	21.6
46.0743	1.96842	0.2476	(-112)	22.1
48.5747	1.87278	0.4772	(-202)	15.5
53.2639	1.71843	0.609	(020)	11.8
58.0454	1.58773	0.5988	(202)	12.5
61.3365	1.51019	0.5072	(-113)	15.8
66.0906	1.41261	0.4723	(-311)	18.3
67.7928	1.38122	0.6378	(113)	13.3
72.155	1.30808	0.591	(311)	11.9
74.8743	1.26717	0.669	(004)	13.1

The R. stricta contains several phytochemicals such as tannins, saponins, alkaloids, steroids, flavonoids, carbohydrates, cardiac glycosides, quinones, glycosides, terpenoids, phenols, and others [37]. Copper hydroxide (Cu $(OH)_2$) is first formed when the metal precursor ($Cu(NO_3)_2$:$3H_2O$) interacts with the hydroxyl anion (–OH) produced by water. Numerous phytochemical components found in R. stricta's aqueous extract function as encapsulating agents and reduce copper hydroxide to copper oxide nanoparticles. FTIR is one of the most important techniques to identify the function groups of materials. Fig. 4 shows that the FTIR bands located at 1417.68 cm^{-1} corresponds to O-H bending, 1109.07cm^{-1} is attributed to C-O, 1058.92 cm^{-1} is attributed to the C-H stretching vibrations, 873.75cm^{-1} is attributed to aromatic C–H bending, whereas the peaks at 615.29 cm^{-1}, 530.42, 482.20 and 418.55 cm^{-1} can be attributed to vibrations of CuO, confirming the formation of CuONPs [38, 39].

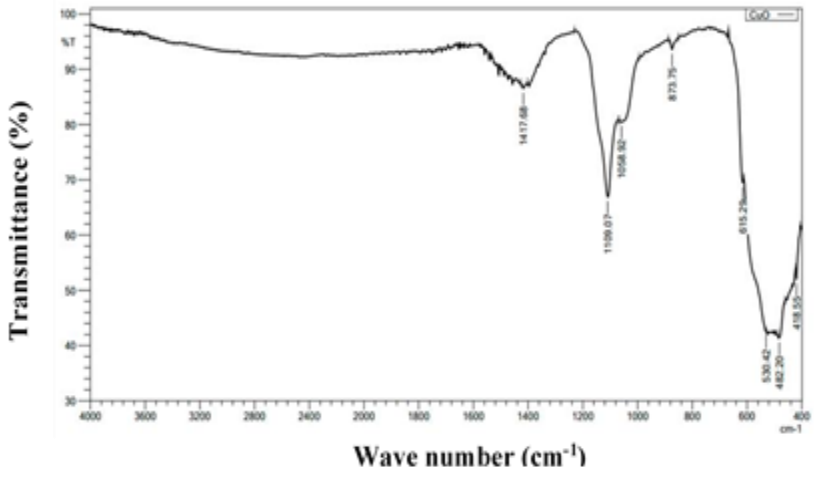

Figure 4: FTIR spectrum of CuONPS synthesized using R. stricta leaves extract.

Fig.5 shows the UV-Vis absorption spectrum of the green synthesized CuONPs using R. stricta leaves extract. The absorption peaks were revealed at 280 nm. The

observed spectrum can be attributed to the surface Plasmon resonances of CuONPs. The outermost layer of plasmons is absorbed by metal oxide nanoparticles because of the coordinated oscillation of free electrons in the conduction band, which is speeded up by electromagnetic radiation coming in. The wavelength of the incident light exceeds the particle diameter, resulting in the observation of this type of resonance. The surface plasmon absorption bands at 280 nm indicate the formation of CuONPs. This results in agreements with that of Priya et al. [40]. The energy gap (E_g) was determined using a Tauc plot, as shown in Fig. 5, and the corresponding equation given below [41]:

$$(\alpha h\nu)^2 = (h\nu - E_g) \quad (3)$$

where: α is the absorption coefficient, $h\nu$ is the photon energy. Fig. 5 shows direct transition and a band gap value of 3.9 eV for CuONPs. The larger band gap value of CuONPs compared to E_g = 1.9 eV of the bulk CuO [42] can be attributed to the quantum confinement effect [43]. Larger band gap values are associated with nanoparticles. The varying capacities of phytochemicals found in the plant extracts used for reduction and stabilization during the synthesis process may cause of the modest increase in the band gap value of CuONPs. This outcome is consistent with the results of Lakshmanan et al. [44].

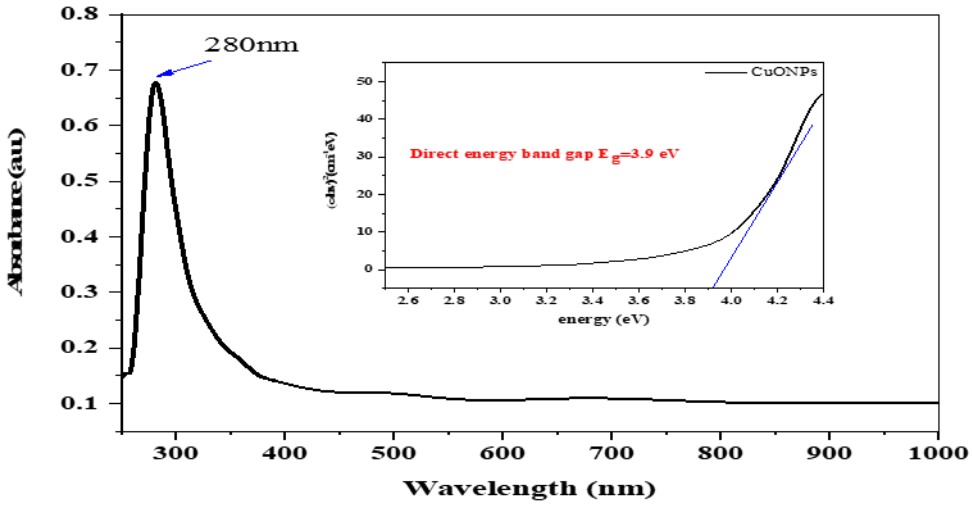

Figure 5: UV-Visible spectrum of CuONPs and the optical energy band gap.

Zeta potential provides the zeta value, which shows the surface charge and stability of CuONPs prepared using R. stricta leaves extract. A zeta potential value within the range of (± 40 to ± 60) mV indicates good stability. The zeta value of the synthesized CuONPS was -49.7 mV, as shown in Fig. 6, indicating good stability [45]. Snehal Yedurkar et al. [46] concluded that "if the particles in a suspension have large negative or positive (zeta- potential values, particles will repel each other and there will be no aggregation of NPs. On the other hand, if particles have small zeta-potential values, there is no force to prevent particles from coming together and aggregating".

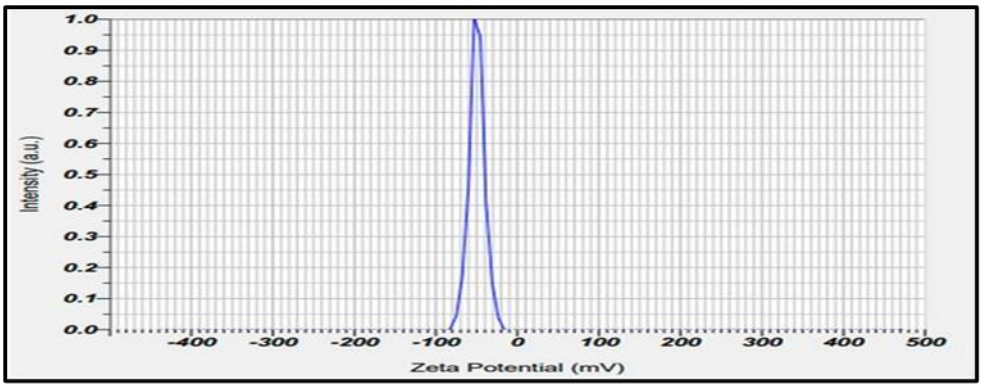

Figure 6: Zeta potential of CuONPs synthesized using R. stricta leaves extract.

3.1. Antibacterial Activity

The antibacterial efficiency of the CuONPs synthesized using R. stricta leaves extract was assessed using the well diffusion method on Mueller-Hinton Agar (MHA). The MHA agar plates were subjected to aseptic conditions and inoculated with the test bacterial strain. Wells with a diameter of 6mm were filled with different concentrations of (100, 200, 400, and 800µg/l) of the nanoparticle. The plates were then incubated at a temperature of 37°C for 24 hrs. The diameter of the inhibition zones was measured in millimeters (mm) after the incubation period.

The study utilized deionized water as the control (A). Nanoparticles with a large surface area to volume ratio are well dispersed and have small crystallite sizes, making it easy for them to interact with the surfaces of microbes. The nanoparticles' expansive surface area enhances their contact with microorganisms, enabling them to perform various antibacterial actions [47]. The gram-positive Staphylococcus aureus bacterium was selected as the subject of the study to investigate the antibacterial properties of CuONPs. This bacterium is a human pathogen that can cause various skin, respiratory system, and cardiovascular infections. Additionally, the gram-negative Klebsiella pneumoniae bacterium was chosen due to the severity of the infection it inflicts, which has high mortality rates even when treated properly [48]. The antibacterial activity of CuONPs synthesized using R. stricta leaves extract against Staphylococcus aureus and Klebsiella pneumonia were evaluated for their role in antibacterial action, as shown in Fig.7 a and b. In general, Fig.7 (a and b) showed that the inhibition zone of CuONPs got larger with increasing the NPs concentration; the largest inhibition zone was observed for the 800µg/l CuONPs concentration. Furthermore, the largest inhibition zone was 30mm against gram-positive Staphylococcus aureus bacteria, as shown in Fig.7b, while it was 21mm for gram-negative Klebsiella pneumonia, as shown in Fig. 7a. An inhibition zone on the plate indicates the absence of bacterial growth. CuO nanoparticles stick to the bacteria and stop them from working normally. They also damage to the bacteria's outer layers, including their DNA, proteins, and lipids [49]. The adhesion and bioactivity between bacteria and CuO ions generated by nanoparticles result from electrostatic forces when the ions are adsorbed onto the surface of the micro-organism's cell wall. This destroys the cell wall by exploiting the microorganism's vulnerability to the nanoparticles, which possess inherent resistance properties against infections. The efficiency of the produced CuO nanoparticles was assessed based on the diameter of the clear zone, with larger diameters indicating higher efficiency [50]. The study demonstrated the efficiency of CuO nanoparticles in eradicating a bacterial pathogen, with excellent antibacterial impact shown at high nanoparticles concentration. The results are consistent with the findings of Khalil et al. [51].

3.2. Anticancer Activity

In pharmaceutical and biomedical applications, the cytotoxicity, cell viability, and biocompatibility of nanoparticles are crucial factors. CuONPs' ease of binding and compatibility with biomolecules make them suitable for use as nanocarriers of anticancer drugs. CuONPs' in vitro cytotoxicity was investigated using the MTT test on A549 cell lines. The purpose of this study was to examine the anticancer activity of CuONPs. A549 lung cancer was chosen as the study subject since lung cancer is a disease that is commonly dreaded and is the primary cause of death worldwide. Previous research has shown that the impact of lung cancer accounts for 17.6% of fatalities and 12.4% of unusable cases [52].

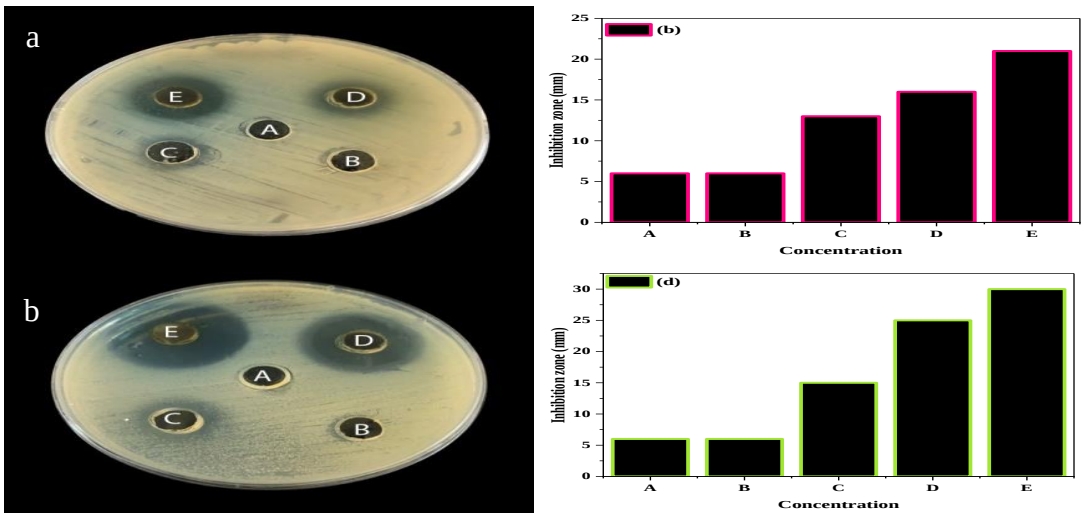

Figure 7: Antibacterial activity of ZnONPs against (a) k.pneumoniae and (b) S. aureus. A the control and with different CuONPs doses (B)100 µg/ml, (C) 200 µg/ml, (D) 400 µg/ml, and (E) 800 µg/ml.

Fig. 8 represents the morphological changes of the cells treated with the synthesized CuONPs compared to the untreated cells (control). CuONPs caused many morphological changes in A549 cells, while no such changes were observed in cells that were not treated. As seen in Fig. 8, these morphological changes included changes in cell form, clumping, blockage of cell communication, and chromatin condensation in A549 cells that experienced cell death. In contrast, the untreated cells remained active. The results indicated that exposing A549 cells to different concentrations of CuONPs for 48 hrs significantly reduced the cell viability at the higher concentration of 100 µg/ml. As the CuONPs concentration increased, the cell survivability decreased considerably. When A549 cells were exposed to CuONPs of 6.52 ,12.5, 25, 50, and 100 µg/ml concentrations, the cytotoxicity increased significantly from 12.10±1.626 to 81.47±1.517 as shown in Figure 9. The viability of the treated cell line was dose-dependent, indicating that higher concentrations of CuONPs have higher toxicity toward the cancer cell line. The properties of NPs, such as nanoparticle size, surface charge, and functional groups, which dictate NPs' therapeutic potential, may be the cause of CuONPs' cytotoxic effects [53]. CuONPs with smaller NP sizes have superior pharmacological and biomedical capacities, according to a recent study [54]. It is also possible that the elevated levels of reactive oxygen species (ROS) produced in the membrane caused phospholipids in the membrane to be attacked by free radicals, which resulted in a loss of membrane integrity and the induction of apoptosis with fragmented nuclei. The activation of apoptosis is aided by the upregulated ROS level in cancer cells, which also modifies mitochondrial activities [55, 56].

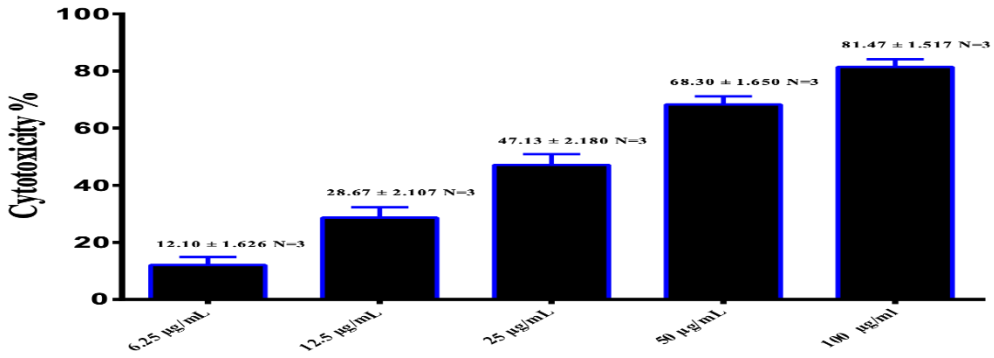

Figure 8: Morphological changes in A549 cancer cells of (a) untreated and (b) treated with synthesized CuONPs from R. stricta leaves extract.

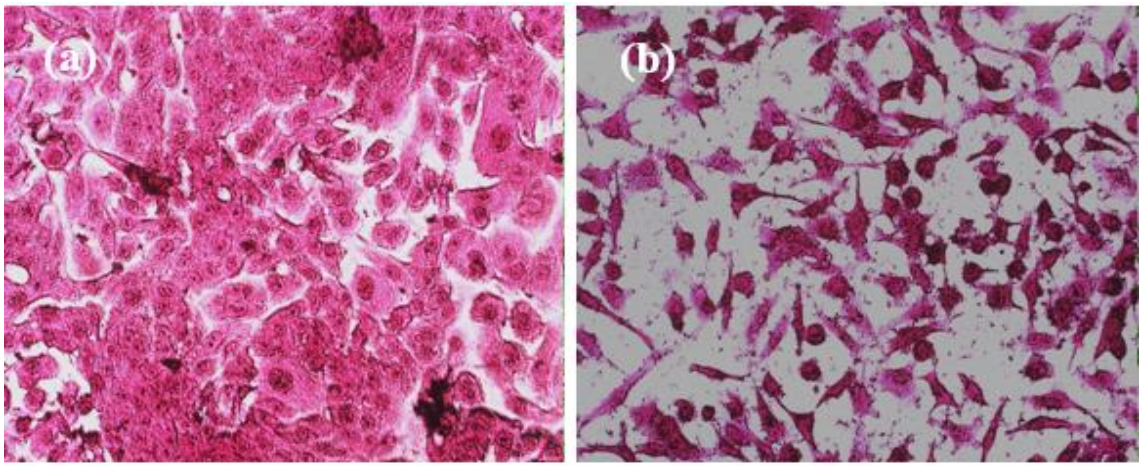

Figure 9: Cytotoxicity of CuONPs against A549 cell line.

4. Conclusions

Copper oxide nanoparticles (CuONPs) were successfully synthesized using an aqueous leaf extract of R.stricta. This method, characterized by its simplicity, rapidity, ease, and eco-friendly approach, involved bioactive molecules within the leaves acting as both reducing and stabilizing agents for NP formation. The XRD analysis unveiled a monoclinic structure. FESEM illustrated a semi-spherical and cubic shape. The surface charge exhibited positivity, ensuring excellent stability at -49.7mV. CuONPs demonstrated significant biological activities, including antibacterial and cytotoxic effects. The largest inhibition zone, measuring 30 mm, was observed against the gram-positive bacterium S. aureus, while it measured 21 mm against gram-negative bacteria. A dose-dependent cytotoxic effect was apparent, with higher concentrations of CuONPs corresponding to increased cytotoxicity, specifically measuring 81.47 ± 1.517. These findings suggest that CuONPs synthesized from the aqueous extract of leaves have the potential to function as a natural antibacterial and anticancer agent.

Conflict of interest

Authors declare that they have no conflict of interest.

References

1. H. H. Ali and F. T. M. Noori, Iraqi J. Appl. Phys. **19**, 59 (2023).
2. E. E. Al-Abodi, Ibn AL-Haitham J. P. Appl. Sci. **36**, 246 (2023). DOI: 10.30526/36.1.2933.

3. S. M. Bhagyaraj, O. S. Oluwafemi, N. Kalarikkal, and S. Thomas, *Synthesis of Inorganic Nanomaterials* (Duxford, United Kingdom, Woodhead Publication, 2018).
4. N. M. Ishak, S. Kamarudin, and S. Timmiati, Mat. Res. Exp. **6**, 112004 (2019). DOI: 10.1088/2053-1591/ab4458.
5. K. N. Thakkar, S. S. Mhatre, and R. Y. Parikh, Nanomedic. Nanotech. Bio. Medic. **6**, 257 (2010). DOI: 10.1016/j.nano.2009.07.002.
6. G. Singhal, R. Bhavesh, K. Kasariya, A. R. Sharma, and R. P. Singh, J. Nanopart. Res. **13**, 2981 (2011). DOI: 10.1007/s11051-010-0193-y.
7. M. Hudlikar, S. Joglekar, M. Dhaygude, and K. Kodam, J. Nanopart. Res. **14**, 1 (2012). DOI: 10.1007/s11051-012-0865-x.
8. K. Govindaraju, S. K. Basha, V. G. Kumar, and G. Singaravelu, J. Mat. Sci. **43**, 5115 (2008). DOI: 10.1007/s10853-008-2745-4.
9. M. F. Lengke, M. E. Fleet, and G. Southam, Langmuir **23**, 2694 (2007). DOI: 10.1021/la0613124.
10. M. Kowshik, N. Deshmukh, W. Vogel, J. Urban, S. K. Kulkarni, and K. Paknikar, Biotech. Bioeng. **78**, 583 (2002). DOI: 10.1002/bit.10233.
11. D. Rautaray, A. Ahmad, and M. Sastry, J. American Chem. Soci. **125**, 14656 (2003). DOI: 10.1021/ja0374877.
12. Anshup, J. S. Venkataraman, C. Subramaniam, R. R. Kumar, S. Priya, T. S. Kumar, R. Omkumar, A. John, and T. Pradeep, Langmuir **21**, 11562 (2005). DOI: 10.1021/la0519249.
13. S. Honary, H. Barabadi, E. Gharaei-Fathabad, and F. Naghibi, Dig. J. Nanomat. Biostruc. **7**, 999 (2012).
14. K. Gebremedhn, M. H. Kahsay, and M. Aklilu, J. Pharm. Pharm. **7**, 2328 (2019). DOI: 10.17265/2328-2150/2019.06.007
15. V. U. Siddiqui, A. Ansari, R. Chauhan, and W. A. Siddiqi, Mat. Today Proce. **36**, 751 (2021). DOI: 10.1016/j.matpr.2020.05.504.
16. A. Venkatramanan, A. Ilangovan, P. Thangarajan, A. Saravanan, and B. Mani, Curr. Biotech. **9**, 304 (2020). DOI: 10.2174/2211550109999201113095459.
17. F. Marabelli, G. Parravicini, and F. Salghetti-Drioli, Phys. Rev. B **52**, 1433 (1995). DOI: 10.1103/PhysRevB.52.1433.
18. A. El-Trass, H. Elshamy, I. El-Mehasseb, and M. El-Kemary, Appl. Surf. Sci. **258**, 2997 (2012). DOI: 10.1016/j.apsusc.2011.11.025.
19. G. Filipič and U. Cvelbar, Nanotechnology **23**, 194001 (2012). DOI:10.1088/0957-4484/23/19/194001.
20. J. Li, F. Sun, K. Gu, T. Wu, W. Zhai, W. Li, and S. Huang, Appl. Catal. A Gen. **406**, 51 (2011). DOI: 10.1016/j.apcata.2011.08.007.
21. J. Chen, S. Mao, Z. Xu, and W. J. Ding, RSC Advances **9**, 3788 (2019). DOI: 10.1039/C8RA09186B.
22. S. Sathiyavimal, S. Vasantharaj, D. Bharathi, M. Saravanan, E. Manikandan, S. S. Kumar, and A. Pugazhendhi, J. Photochem. Photobio. B Bio. **188**, 126 (2018). DOI: 10.1016/j.jphotobiol.2018.09.014.
23. B. Turakhia, M. B. Divakara, M. S. Santosh, and S. Shah, J. Coat. Tech. Res. **17**, 531 (2020). DOI: 10.1007/s11998-019-00303-5.
24. A. Ahmad and S. Gadgeel, *Lung Cancer and Personalized Medicine: Current Knowledge and Therapies* (Switzerland Springer Cham, 2015).
25. D. P. Carbone, M. Reck, L. Paz-Ares, B. Creelan, L. Horn, M. Steins, E. Felip, M. M. Van Den Heuvel, T.-E. Ciuleanu, and F. Badin, New England J. Med. **376**, 2415 (2017). DOI: 10.1056/NEJMoa1613493.
26. R. Seigneuric, L. Markey, D. Sa Nuyten, C. Dubernet, C. Ta Evelo, E. Finot, and C. Garrido, Curr. Molec. Med. **10**, 640 (2010). DOI: 10.2174/156652410792630634.
27. R. Khan, M. N. Baeshen, K. S. Saini, R. S. Bora, A. M. Al-Hejin, and N. A. Baeshen, Biotech. Biotech. Equip. **30**, 1016 (2016). DOI: 10.1080/13102818.2016.1209087.
28. B. Al-Dabbagh, I. A. Elhaty, A. A. Al Hrout, R. Al Sakkaf, R. El-Awady, S. S. Ashraf, and A. Amin, BMC Complem. Alternat. Med. **18**, 240 (2018). DOI: 10.1186/s12906-018-2285-7.
29. Y. B. Chan, V. Selvanathan, L.-H. Tey, M. Akhtaruzzaman, F. H. Anur, S. Djearamane, A. Watanabe, and M. Aminuzzaman, Nanomaterials **12**, 3589 (2022). DOI: 10.3390/nano12203589
30. K. Pakzad, H. Alinezhad, and M. J. Nasrollahzadeh, Ceram. Int. **45**, 17173 (2019). DOI: 10.1016/j.ceramint.2019.05.272.
31. A. Atri, M. Echabaane, A. Bouzidi, I. Harabi, B. M. Soucase, and R. B. Chaâbane, Heliyon **9**, (2023). DOI: 10.1016/j.heliyon.2023.e13484.
32. E. Nasir, M. Alias, and A. M. Ali, IOP Conference Series: Materials Science and Engineering (IOP Publishing, 2020). p. 012053.

33. M. H. Suhail, I. K. Adehmash, S. M. Abdul Kareem, D. A. Tahir, and O. G. Abdullah, Transact. Electric. Elect. Mat. **21**, 355 (2020). DOI: 10.1007/s42341-020-00182-3.
34. N. K. Abbas, Baghdad Sci. J. **20**, 1779 (2023). DOI: 10.21123/bsj.2023.7290.
35. H. R. Naika, K. Lingaraju, K. Manjunath, D. Kumar, G. Nagaraju, D. Suresh, and H. Nagabhushana, J. Taibah Univ. Sci. **9**, 7 (2015). DOI: 10.1016/j.jtusci.2014.04.006.
36. S. Rehman, N. A. Shad, M. M. Sajid, K. Ali, Y. Javed, Y. Jamil, M. Sajjad, A. Nawaz, and S. K. Sharma, Iran. J. Chem. Chem. Eng **41**, 1549 (2022). DOI: 10.30492/IJCCE.2021.127597.4127.
37. R. Mahmood, F. Malik, S. Shamas, T. Ahmed, M. Kausar, S. Rubnawaz, M. Ashfaq, S. Hussain, B. D. Green, and B. J. Mirza, Bolet. Latinoam. y del Car. de Plan. Med. y Aromat. **19**, 188 (2020).
38. A. Varughese, R. Kaur, and P. Singh, IOP Conference Series: Materials Science and Engineering (IOP Publishing, 2020). p. 012011.
39. F. Amin, Fozia, B. Khattak, A. Alotaibi, M. Qasim, I. Ahmad, R. Ullah, M. Bourhia, A. Gul, and S. Zahoor, Evid. Bas. Complem. Alternat. Med. **2021**, 5589703 (2021). DOI: 10.1155/2021/5589703.
40. M. Priya, R. Venkatesan, S. Deepa, S. S. Sana, S. Arumugam, A. M. Karami, A. A. Vetcher, and S.-C. Kim, Sci. Rep. **13**, 18838 (2023). DOI: 10.1038/s41598-023-46002-5.
41. J. H. Taha, N. K. Abbas, and A. A. Al-Attraqchi, Baghdad Sci. J. **20**, 1146 (2023). DOI: 10.21123/bsj.2023.7294.
42. M. Kaur, K. P. Muthe, S. K. Despande, S. Choudhury, J. B. Singh, N. Verma, S. K. Gupta, and J. V. Yakhmi, J. Crys. Grow. **289**, 670 (2006). DOI: 10.1016/j.jcrysgro.2005.11.111.
43. N. R. Dhineshbabu, V. Rajendran, N. Nithyavathy, and R. Vetumperumal, Appl. Nanosci. **6**, 933 (2016). DOI: 10.1007/s13204-015-0499-2.
44. S. P. Lakshmanan, S. T. Jostar, G. J. Arputhavalli, S. Jebasingh, and C. M. R. Josephine, Int. J. Nanosci. Nanotech. **17**, 109 (2021).
45. A. A. Barzinjy and H. H. Azeez, SN Appl. Sci. **2**, 991 (2020). DOI: 10.1007/s42452-020-2813-1.
46. S. Yedurkar, C. Maurya, P. Mahanwar, and Applications, Open J. Synth. Theo. **5**, 1 (2016). DOI: 10.4236/ojsta.2016.51001.
47. R. Nallendran, G. Selvan, and A. R. Balu, Surf. Interf. **15**, 11 (2019). DOI: 10.1016/j.surfin.2019.02.002.
48. J. V. Ashurst and A. Dawson, *Klebsiella Pneumonia* (USA, StatPearls Publishing LLC, 2023).
49. F. Ijaz, S. Shahid, S. A. Khan, W. Ahmad, and S. Zaman, Tropic. J. Pharmaceut. Res. **16**, 743 (2017). DOI: 10.4314/tjpr.v16i4.2.
50. A. Vala and S. Shah, Int. J. Nanosci. Nanotech. **8**, 197 (2012).
51. M. M. Khalil, E. H. Ismail, K. Z. El-Baghdady, and D. Mohamed, Arabian J. Chem. **7**, 1131 (2014). DOI: 10.1016/j.arabjc.2013.04.007.
52. D. B. Manikandan, M. Arumugam, S. Veeran, A. Sridhar, R. Krishnasamy Sekar, B. Perumalsamy, and T. Ramasamy, Envir. Sci. Pollut. Res., 1 (2021). DOI: 10.1007/s11356-020-12108-w.
53. I. Khan, K. Saeed, and I. Khan, Arabian J. Chem. **12**, 908 (2019). DOI: 10.1016/j.arabjc.2017.05.011.
54. A. Abbasi, K. Ghorban, F. Nojoomi, and M. Dadmanesh, Asian Pacif. J. Canc. Prevent. APJCP **22**, 893 (2021). DOI: 10.31557/APJCP.2021.22.3.893.
55. Y.-H. Ling, L. Liebes, Y. Zou, and R. Perez-Soler, J. Bio. Chem. **278**, 33714 (2003). DOI: 10.1074/jbc.M302559200.
56. L. Gibellini, M. Pinti, M. Nasi, S. De Biasi, E. Roat, L. Bertoncelli, and A. Cossarizza, Cancers **2**, 1288 (2010). DOI: 10.3390/cancers2021288.

التوليف الأخضر للجسيمات النانوية CuO بوساطة مستخلص أوراق نبات حرمل الرازي توصيف وتقييم نشاطها المضاد للبكتيريا ونشاطها المضاد للسرطان (دراسة مخبرية)

عبير محمد مسلم[1،2] واقبال سهام ناجي[1]
[1]قسم الفيزياء، كلية العلوم، جامعة بغداد، بغداد، العراق
[2]جامعة ابن سينا للعلوم الطبية والصيدلانية، بغداد، العراق

الخلاصة

تم في هذه الدراسة استخدم طريقة مباشرة وسريعًة وصديقًة للبيئة لتصنيع جزيئات أكسيد النحاس النانوية باستخدام مستخلص مائي من أوراق حرمل الرازي. خضعت جسيمات اكسيد النحاس النانوية المميزة لفحص شامل من خلال تقنيات تحليلية مختلفة، بما في ذلك تحليلات XRD، وFESEM، وEDX، والتحليل الطيفي للأشعة فوق البنفسجية، وFT-IR، والجهد السطحي zeta potential. أثبت تحليل XRD الطبيعة البلورية أحادية الميل، وكشف عن متوسط حجم بلوري يبلغ 15.6 نانومتر. صورت صور FESEM أشكالًا شبه كروية ومكعبية، بأحجام جسيمات تتراوح من 56.64 إلى 86.95 نانومتر. تم تأكيد تكوين جسيمات اكسيد النحاس النانوية في البداية من خلال التغير الملحوظ في اللون، والذي يعزى إلى إثارة رنين البلازمون السطحي عند 280 نانومتر في أطياف الأشعة فوق البنفسجية. أكد تحليل FTIR وجود مجموعات وظيفية في مستخلص أوراق حرمل الرازي، تعمل كعوامل اختزال وتثبيت، مما يسهل تكوين جسيمات اكسيد النحاس النانوية. أشارت قياسات الجهد السطحي إلى استقرارية كبيرة بقيمة 49.7- ملي فولت. تم تقييم الجسيمات النانوية المُصنّعة حيويًا لخصائصها المضادة للبكتيريا ضد الكليبسيلا الرئوية والمكورات العنقودية الذهبية، مما أدى إلى مناطق تثبيط تبلغ 21 ملم و30 ملم على التوالي. بالإضافة إلى ذلك، كشف تقييم السمية لـجسيمات اوكسيد النحاس النانوية ضد خطوط الخلايا A549 عن سمية عالية قدرها 81.47 ± 1.517 بتركيز 100 ميكروغرام / مل. هذه هي المحاولة الأولى لتخليق جسيمات اوكسيد النحاس النانوية من حرمل الرازي كعوامل مضادة للبكتيريا ومضادة للسرطان ويمكن استغلالها لاحقًا كمرشح محتمل لعامل مضاد للبكتيريا ومضاد للسرطان ويمكن استخدامه بعد إجراء مزيد من الدراسات على الجسم الحي.

الكلمات المفتاحية: اوكسيد النحاس، الجسيمات النانوية، حرمل الرازي، فعالية مضادة للبكتيريا، فعالية مضادة للسرطان.